JOURNAL OF SOLID STATE CHEMISTRY 116, 232–239 (1995)

Defect Chemistry of $CaSO_4$ Added to Ag_2SO_4

K. Singh,*,[1] S. M. Pande,† and S. S. Bhoga‡

*Department of Physics, Nagpur University Campus, Amravati Road, Nagpur 440010, India; †Department of Applied Physics, RKN Engineering College, Nagpur 440013, India; and ‡Department of Physics, Hislop College, Nagpur 440001, India

Received May 24, 1994; accepted September 7, 1994

The compositions $(1 - x)Ag_2SO_4$–$(x)CaSO_4$ ($x = 0.01$ to 0.20) are prepared by slow cooling of a melt and also by quenching using a twin roller technique. The solid solubility limit of Ca^{2+} is determined using X-ray powder diffraction and scanning electron microscopy. Conductivity studies, using a detailed impedance analysis, are carried out in low as well as high temperature regions encompassing both the structural modifications of Ag_2SO_4. In the high temperature region ($T > 417$°C), the conductivity is found to be maximal at a 7% vacancy concentration of $CaSO_4$ added to Ag_2SO_4. However, in the low temperature orthogonal phase, a decrease in conductivity within and above the solid solubility limit is observed. The concept of lattice distortion (contraction) due to partial substitution of Ag^+ by Ca^{2+} is introduced to explain a decrease in conductivity in the orthogonal phase. Interfacial reactions and surface defect chemistry are applied to understand the fall in conductivity in $CaSO_4$ dispersed in Ag_2SO_4.

INTRODUCTION

Several attempts have been made in the past to enhance ionic conductivity in polycrystalline solids. In this effort the following basic approaches have been adopted: (i) aliovalent substitution of conducting cations (1, 2), (ii) opening of the lattice structure by wrong size ion substitution (3, 4), (iii) optimization of the preparative parameters (5), (iv) trapping of high temperature highly conducting phases at room temperature (6, 7), (v) stabilization of an open channel structure (8), and (vi) dispersion of an insoluble second phase (9, 10). The first two approaches have been important not only for the development of electrolytes, but also from the point of view of fundamental knowledge.

According to Höfer *et al.* (1), conductivity is strongly correlated to vacancy concentration, whereas the size and the electronic configuration of the substituting ions have no effect. Their studies were, however, confined to high temperatures. In contrast, the dependence of conductivity on aliovalent ionic size and charge has been reported elsewhere (2, 11).

Sulfate based solid electrolytes have potential applications in SO_x gas sensors (12, 13). Among others, silver sulfate is the least attended to. Moreover, the low and high temperature phases of Ag_2SO_4 are isomorphous to those of $CaSO_4$. The partial replacement of Ag^+ by Ca^{2+} is made with a view to distorting the host lattice while creating extrinsic vacancies on the basis of the following formula:

$$Ag_{2-2x}Ca_x\square_xSO_4.$$

EXPERIMENTAL

The initial ingredients, Ag_2SO_4 and $CaSO_4$, with purity greater than 99% were procured from E. Merck (India). Appropriate mole fractions of the above chemicals were prepared by melting the mixture followed by twin roller quenching as discussed earlier (12). The samples were also prepared by taking an appropriate mole fraction of the ingredients into translucent silica ampules (to avoid photo reduction of Ag_2SO_4) and heated in an electrical furnace to temperature 675°C (nearly 20°C above the melting point of pure Ag_2SO_4). Later, the melt was cooled slowly to room temperature at 1.5°C/min. The ingots obtained by breaking the ampules were pulverized to obtain a fine powder.

Thus prepared samples were characterized by X-ray powder diffraction (Philips PW 1700 diffractometer with PW 1710 diffractometer controlling unit) using CuKα radiation. The microstructures were examined with the help of a Cambridge 250 Mark III stereoscan electron microscope.

For electrical conductivity measurements the samples were obtained in the form of circular discs of 9 mm in diameter and 1.5 mm thick by pressing the powder in a Specac (UK) make stainless steel die-punch and hydraulic press. A good ohmic contact was ensured by using high quality graphite paint (Elecleck, India) followed by baking at 200°C for an hour. A Keithley 617 programmable elec-

[1] To whom correspondence should be addressed.

0022-4596/95 $6.00

trometer was used to measure the surface resistance of the coated surface, which was found to be approximately 1 ohm. The entire process was carried out in a dark room. The pellets of quenched samples were sintered at 400°C for 12 hr prior to being spring loaded between the silver electrodes of a sample holder.

Prior to impedance measurements, the spring loaded sample was heated at 440°C for 2 hr in order to homogenize the charge carriers in the sample and simultaneously to remove the moisture content therein. Later, the temperature of the furnace was reduced by steps of 20°C at a cooling rate of 1°C per minute. At the end of each cycle the sample was allowed to attain thermal equilibrium for a dwell time of 40 min using a Eurotherm (UK) PID temperature controller. During this cooling process, the real and imaginary parts of the impedance of the sample were measured as functions of frequency in the range from 5 Hz to 13 MHz and of temperature from 450 to 200°C at the end of each dwell time with the help of a HP 4192A LF impedance analyzer. The HP 16048 test leads were used for electrical connections from the sample to the analyzer to avoid any parasitic impedance due to improper connecting cables. In order to obtain the correct temperature of the sample, the tip of a precalibrated standard Chromel–Alumel thermocouple was kept in close proximity to the sample. The emf of the thermocouple was measured using a Keithley 617 electrometer. The entire measurement system was properly shielded. The reproducibility of the impedance data was confirmed by repeating the measurement on freshly prepared samples. The transport number was determined by the Wagner dc polarization method with the help of a Keithley 236 source measure unit.

RESULTS AND DISCUSSION

All the quenched samples showed time dependent behavior, resulting in 10–20% variation in conductivity during the initial 24–48 hr after they were fast-cooled from the melting temperature for the first time. On subsequent cycling, the conductivity data were reproducible within experimental error (less than ±2%) for various heating and cooling cycles.

It is a well-known fact that, upon fast quenching, apart from the reduction in particle size and the extension of solid solubility, metastable defects are induced (5, 14). These together contribute substantially to improvement in the ionic conductivity of a solid electrolyte. However, when these very samples undergo various temperature cycles during the conductivity measurements or otherwise, the defects caused by "fast-quenching" settle down following the release of stress energy in the given system and the samples attain thermodynamic equilibrium (15).

The same effect could also be achieved by subjecting the quenched samples to sintering, annealing, slow-cooling, or combinations of these. Thus, it is found that samples prepared by rapid quenching and slow cooling techniques behave identically (within experimental error) so far as ionic conductivity in thermodynamically stable samples is concerned.

Diffraction patterns were recorded for samples with 5.27 mol% $CaSO_4$ in Ag_2SO_4 prepared by two different techniques in order to set the solid solubility limit:

(1) Initial ingredients Ag_2SO_4 and $CaSO_4$ in a 0.9473 : 0.0527 ratio were mechanically mixed thoroughly under acetone for 2 hr;

(2) The melt was quenched as described elsewhere (11).

Table 1 displays the experimental d (Å) and relative intensity values for compositions with $x = 0.0527$, 0.0757, 0.100, and 0.139 along with the JCPDS for pure $CaSO_4$ and Ag_2SO_4. It is seen that the experimental d values of the sample (0.9473 Ag_2SO_4–0.0527 $CaSO_4$) prepared by the first technique are in good agreement with those of the JCPDS data for Ag_2SO_4 and $CaSO_4$, whereas I/I_0 values corresponding to $CaSO_4$ are lower than those of the JCPDS. It is worth noting that in the X-ray diffraction pattern of 0.9473 Ag_2SO_4–0.0527 $CaSO_4$, no single line corresponding to $CaSO_4$ is observed, whereas all the experimental lines are found to be in good agreement with the JCPDS data for Ag_2SO_4. The absence of lines corresponding to $CaSO_4$ for this composition indicates the formation of a solid solution. Similar results are found for the compositions with $x < 0.0527$. From Table 1 it is also evident that when the dopant concentration (x) is increased to 0.0757, very few weak lines corresponding to $CaSO_4$ are observed. The samples ($x > 5.27$), in general, show strong lines corresponding to Ag_2SO_4 and very weak ones for the $CaSO_4$ phase.

The small deviations in d values for Ag_2SO_4 can be attributed to the partial replacement of Ag^+ by the smaller Ca^{2+}, since such a replacement results in local distortions (16).

Generally, in X-ray powder diffraction results for the two phase mixture, the relative intensity (I/I_0) values of each phase depend on its concentration; i.e., the higher the concentration of a particular phase, the higher will be the relative intensity for that phase, and vive versa (3). Hence, the larger variations in the values of relative intensity of experimental lines corresponding to $CaSO_4$ are due to the change in the concentration of $CaSO_4$ (as a result of the formation of a solid solution). Thus, the increase in values of I/I_0 corresponding to $CaSO_4$ after $x = 0.0527$ is due to its precipitation in the Ag_2SO_4 matrix, thus leading to phase separation.

Table 2, displaying lattice cell constants (obtained using a PDP11 computer program), shows that the host Ag_2SO_4 lattice undergoes an appreciable contraction upon Ca^{2+} addition within the solid solubility limit.

TABLE 1
Comparison of XRD and JCPDS Data for $x = 0.0527$, 0.0757, 0.100, and 0.184

Mechanically mixed Ag–Ca5.27 m%		Quenched Ag–Ca5.27 m%		Quenched Ag–Ca7.57 m%		Quenched Ag–Ca10 m%		Quenched Ag–Ca18.4 m%		JCPDS[a]			
d_{OBS}	I/I_0	d_{OBS}	I/I_0	d_{OBS}	I/I_0	d_{OBS}	I/I_0	d_{OBS}	I/I_0	d	I/I_0	Phase	(hkl)
4.72	7	4.72	10	4.70	10	4.73	10	4.71	9	4.70	10	Ag	(111)
4.00	8	3.99	23	3.99	24	4.01	20	3.98	20	3.99	25	Ag	(220)
3.51	25	—	—	3.51	2	3.51	13	3.49	19	3.49	100	Ca	(002)
3.18	48	3.18	76	3.18	91	3.18	85	3.17	72	3.17	70	Ag	(040)
2.87	100	2.87	100	2.87	100	2.88	100	2.87	100	2.87	100	AG	(040)
2.87	100	2.87	100	2.87	100	2.88	100	2.87	100	2.87	100	Ag	(311)
2.65	36	2.65	68	2.64	50	2.65	64	2.64	71	2.64	90	Ag	(022)
2.53	13	2.53	12	2.53	19	2.53	13	2.53	12	2.53	17	Ag	(202)
242	11	2.42	26	2.42	20	2.43	21	2.42	25	2.42	30	Ag	(331)
2.27	4	2.27	6	2.27	7	2.27	8	2.27	5	2.27	8	Ag	(151)
2.20	6	—	—	—	—	2.20	1	2.20	3	2.20	20	Ca	(212)
—	—	—	—	—	—	2.18	6	2.18	8	2.18	8	Ca	(103)
1.98	5	1.98	8	1.98	10	1.98	6	1.98	9	1.98	11	Ag	(242)
1.95	4	—	—	1.95	8	1.95	5	1.95	7	1.95	8	Ag	(260)
—	—	—	—	1.94	5	1.93	7	1.94	9	1.94	4	Ca	(222)
1.92	14	1.92	34	1.92	28	1.92	23	1.92	24	1.92	30	Ag	(351)
1.88	4	1.89	5	1.88	7	1.88	6	1.88	4	1.88	5	Ag	(113)
—	—	—	—	—	—	1.74	3	1.74	N6	1.74	10	Ca	(040)
1.71	9	1.71	13	1.71	12	1.71	12	1.71	13	1.71	17	Ag	(062)
—	—	—	—	—	—	—	—	1.64	5	1.64	14	Ca	(232)
1.54	4	1.54	7	1.54	7	1.54	7	1.54	7	1.54	8	Ag	(371)
—	—	—	—	—	—	—	—	1.49	2	1.49	6	Ca	(214)
1.16	2	—	—	—	—	1.16	2	1.16	3	1.16	2	Ca	(060)

Note. Ag–Cax m% = x mol% $CaSO_4$ added to Ag_2SO_4; Ag = Ag_2SO_4 (orthorhombic); Ca = $CaSO_4$ (orthorhombic).
[a] JCPDS card numbers 27–1403 (Ag_2SO_4) and 6-0226 ($CaSO_4$).

A comparison of microphotographs (Figs. 1a and 1b) reveals that the grain morphology of the host material is more or less unaffected by the small addition of $CaSO_4$; further, no trace of a second phase is visible. This supports, along with the XRD results, the view that $CaSO_4$ is making a solid solution with Ag_2SO_4 up to 5.27 mol%. Thus the compositions up to $x = 0.0527$ could be represented by

$$Ag_{2-2x}Ca_x\square_xSO_4,$$

where □ denotes the vacancy.

IONIC CONDUCTIVITY

The variation of $\log \sigma T$ with $10^3/T$ is displayed in Fig. 2. The break in dc conductivity for all the samples indicates the occurrence of a transition from the orthorhombic to the hexagonal phase. For clarity, the results are divided into two temperature regions:

(i) The high temperature region, HTR (orthorhombic phase), and

(ii) The low temperature region, LTR (hexagonal phase).

The curves representing $\log \sigma T$ versus mol% $CaSO_4$ be-

TABLE 2
Comparison of Lattice Cell Constants Calculated Using the PDP11 Package

Cell constant	JCPDS Ag_2SO_4[a]	Quenched Ag_2SO_4 $x = 0.0$	Quenched Ag_2SO_4 $x = 0.0527$
a (Å)	10.2699	10.663	10.272
b (Å)	12.7069	12.685	12.725
c (Å)	05.8181	05.806	05.818
Cell vol. (Å)^3	759.25	785.32	760.47

[a] JCPDS card number 27-1403 (Ag_2SO_4).

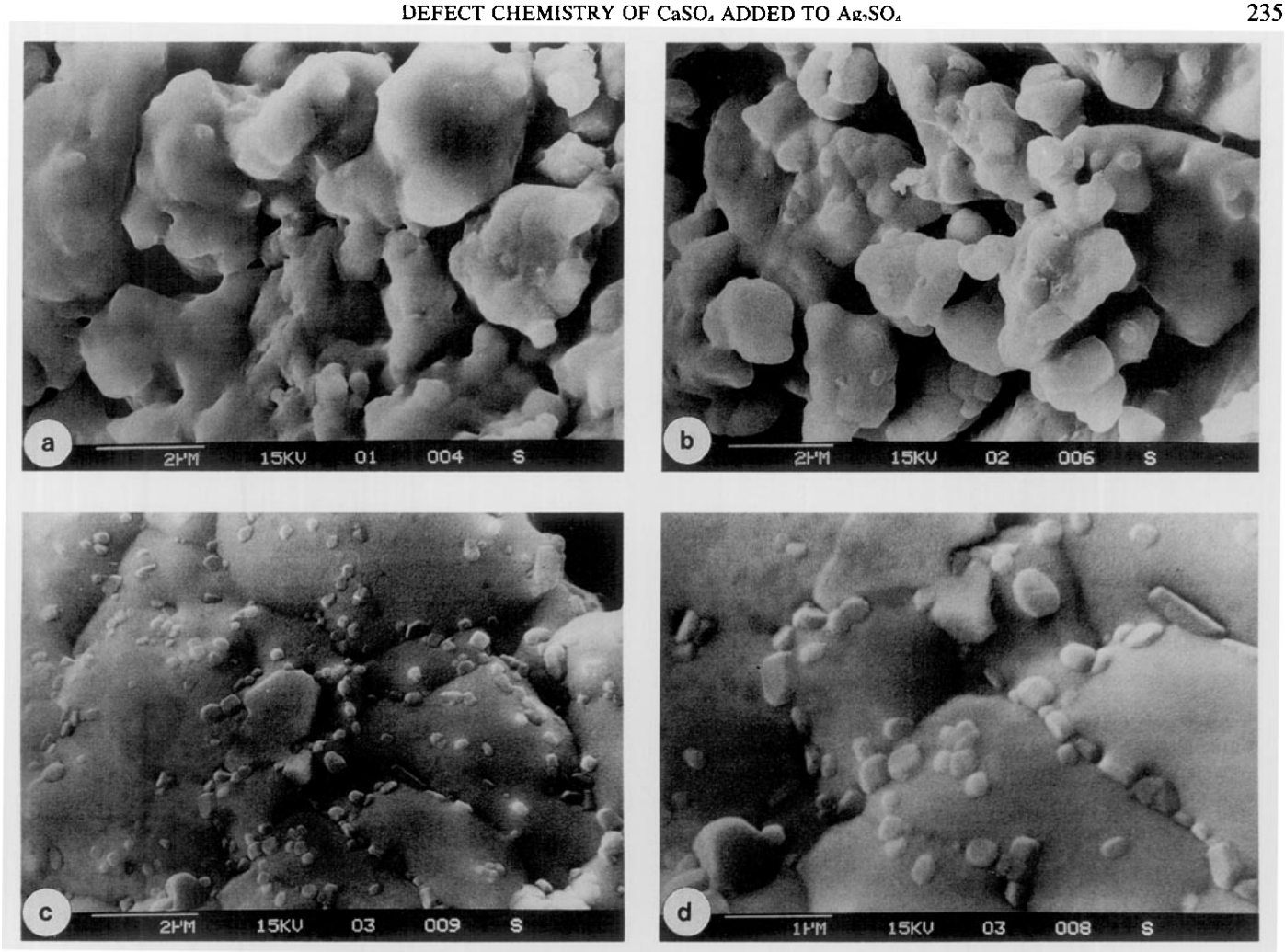

FIG. 1. Microstructures of $(1 - x)$ Ag_2SO_4: (x) $CaSO_4$ for (a) $x = 0.000$, (b) $x = 0.0527$, (c) $x = 0.100$ and (d) exploded view of (c).

havior in these regions are displayed in Figs. 3 and 4a, 4b respectively.

(i) HTR

As seen, in the high temperature region, the conductivity displays a maximum at 7.57 mol% (7% Vac) $CaSO_4$ in Ag_2SO_4 (Fig. 3), which is in total agreement with Hofer's report for Na_2SO_4 (1). The conductivity behavior here could be explained as follows.

The replacement of the host monovalent by the guest divalent ion gives rise to additional vacancies in the host lattice. In the high temperature phase it is reported that such extrinsic vacancies contribute chiefly to the conductivity, whereas the ionic size effect is insignificant following aliovalent dopant substitution in the host lattice (1).

The hexagonal phase being a more open structure, Ag^+ ions squeeze through the lattice with a high elementary hopping probability (18) on account of the availability of additional vacancies created by $CaSO_4$ substitution. With increasing vacancy concentrations due to partial substitution of Ca^{2+}, additional migration paths for Ag^+ are created, which in turn increases the conductivity (Fig. 3). Upon further addition beyond 7% vac concentration, the mobility of the Ag^+ is reduced following vacancy interactions such as cluster formation and also cationic sublattice ordering (1).

(ii) LTR

The conductivity, in this region, is seen to decrease (Fig. 4a) as a function of the added $CaSO_4$ concentration, in sharp contrast to the observations in the high temperature (hexagonal) region. The results in the domain of low temperatures can be understood as follows.

In the low temperature region (LTR), the bulk conduction is mainly governed by ionic size and the valence of the guest substituting cation. Thus this could be termed as an impurity controlled region (19).

The decrease in conductivity in comparison with that

obtained in HTR cannot be understood by the above discussed classical theory of aliovalent doping alone. This theory accounts for the creation of additional vacancies to maintain the charge neutrality, whereby an enhancement in conductivity is generally a foregone conclusion. An extension of this theory is qualitatively discussed here to explain the behaviour of conductivity due to Ca^{2+} substitution.

The partial replacement of the host monovalent Ag^+ by the guest divalent Ca^{2+} gives rise to additional vacancies (in the vicinity of the guest cation) in the host lattice. In this case, the host lattice stays undistorted if the host and the guest cations are of comparable sizes. On the other hand, in general, local lattice distortion takes place when guest cations of the "wrong" size are added to the host (4, 20). In particular, the host lattice expands due to the incorporation of larger ions in lithium sulfate (2, 3), whereas it contracts on smaller guest cation substitution, as evident from the lattice constants shown in Table 2. The model based on the mobility of the ions as a function of extrinsic vacancies in a distorted lattice leads to several structural interpretations. In the simplest case, since the Ca^{2+} has a smaller ionic radius (0.99 Å) than Ag^+ (1.26 Å), the partial replacement of the latter by Ca^{2+} gives rise to additional vacancies along with appreciable lattice contraction (Table 2). This host lattice distortion is in the vicinity of Ca^{2+}; i.e., localized lattice contraction takes place. Moreover, the mobility of the Ag^+ is considerably reduced following a modest vibrational amplitude

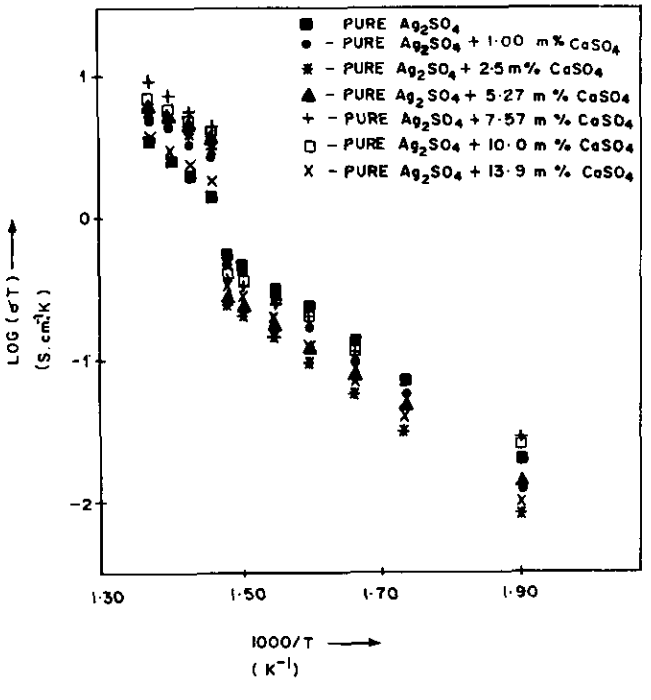

FIG. 2. Variation of $\log(\sigma T)$ with $10^3/T$.

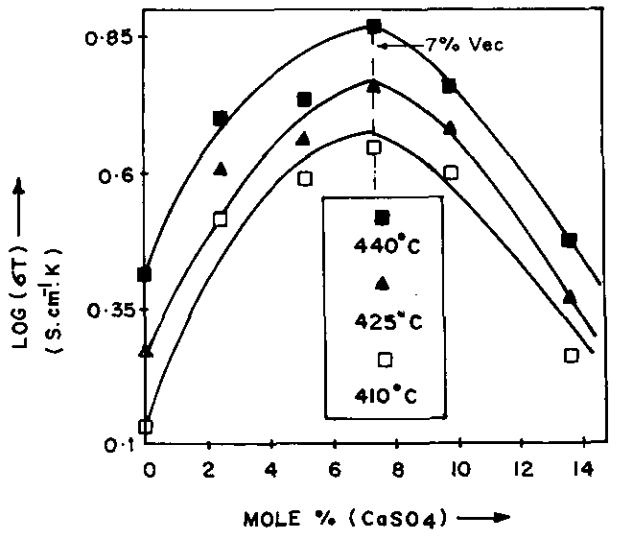

FIG. 3. Variation of $\log(\sigma T)$ with mole% of $CaSO_4$ at high temperatures (HTR).

in the low temperature region. This leads to a decrease in conductivity, which is in good agreement with the results (Fig. 4a).

The above process could also be visualized by considering the host matrix as shown schematically in Fig. 5a. As depicted, the guest Ca^{2+} is partially substituted randomly for Ag^+ (Fig. 5b). In order to attain thermodynamic equilibria (constancy of electrochemical potential, constancy of activity, and hence constancy of electric potential) in the vicinity of Ca^{2+}, (i) an additional vacancy is created and (ii) contraction of the host lattice takes place (Fig. 5b). The disorder reaction can be written using Kroger Vink notation as

$$\mathrm{Ag_{Ag}(Ag_2SO_4)} + x\mathrm{Ca}^{\cdot\cdot} = \{(1-x)\mathrm{Ag_{Ag}(Ag_2SO_4)} + x[\mathrm{Ca_{Ag}(Ag_2SO_4)} + V'_{\mathrm{Ag}}(\mathrm{Ag_2SO_4})]\} \quad [\mathrm{I}]$$

The lattice contraction in the vicinity of Ca^{2+} not only deepens the potential well corresponding to an extrinsic vacancy but also enhances the potential barrier height for nearby mobile ions (Fig. 5). Such an additional vacancy with a deeper potential well offers an appreciable activation energy of migration (E_m) for mobile Ag^+, which in turn contributes to the total activation enthalpy ($E_a = E_f + E_m$) for ion conduction (E_f being the activation enthalpy of defect formation). This decreases the total ionic conductivity in the low temperature region (Fig. 4a). Furthermore, Ca^{2+} being divalent has its own self-trapping effect and therefore is negligibly mobile and impedes the pathways of Ag^+, which is otherwise mobile. Thus the ionic conductivity within the solid solubility region decreases with $CaSO_4$ content.

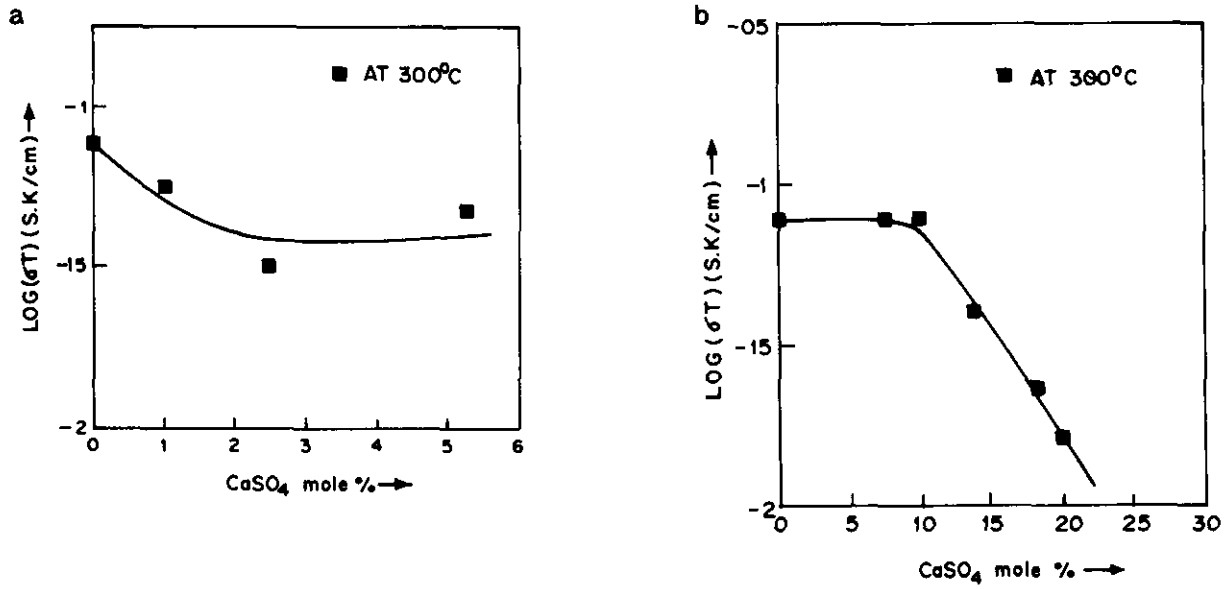

FIG. 4. Variation of $\log(\sigma T)$ with mole% of $CaSO_4$ at 300°C (LTR): (a) within solid solubility, (b) biphase mixture.

As the concentration of $CaSO_4$ is further increased beyond 5.27 mol%, the insoluble phase disperses into the Ag_2SO_4 matrix (Table 1). This could be further supplemented by taking a look at the microphotograph (Fig. 1c)—on further addition of $CaSO_4$ the calcium sulphate grains are seen dispersed throughout the host matrix, thus confirming the phase separation.

In previous investigations, the dispersion of the second insoluble phase is reported to enhance conductivity (10, 21). In contrast to these reports, conductivity of $CaSO_4$ dispersed samples does not exhibit such a trend (Fig. 4b).

According to dispersed phase theory for $MX/M'X$, there is a net transfer of cations from either phase across the interface (14, 22). Two probable Frankel analogue interface reactions are

$$Ag_{Ag}(Ag_2SO_4) + V_i(CaSO_4) = Ag_i^{\cdot}(CaSO_4) + V'_{Ag}(Ag_2SO_4) \quad [II]$$

and

$$V_i(Ag_2SO_4) + Ca_{Ca}(CaSO_4) = Ca_i^{\cdot\cdot}(Ag_2SO_4) + V''_{Ca}(CaSO_4). \quad [III]$$

The corresponding mass action law takes the form

$$C_v C_i = C_0 \exp(-\Delta G^0) \quad [1]$$

where C_v and C_i are the vacancy concentration in one phase and the interstitial concentration in the other, ΔG^0 is free enthalpy for the reaction, and C_0 is the preexponential factor.

If the free energy for reaction [II] exceeds that for reaction [III], this gives rise to additional interstitial Ca^{2+} in Ag_2SO_4, leaving behind equivalent vacancies in the $CaSO_4$ lattice; otherwise the converse is true. Since Ca^{2+} is more electropositive than Ag^+ vis-a-vis antagonist SO_4^{2-}, reaction [III] is thermodynamically more favorable. In addition, as a result of repulsive interaction Ca^{2+} pushes back the surface Ag^+ into the Ag_2SO_4, thus forbiding reaction [II]. These two factors enrich the interstitial ion and vacancy concentrations forming space charge layers close to the Ag_2SO_4 and $CaSO_4$ surfaces, respectively (Fig. 6a).

The enhanced defect concentration is given by

$$C_v/C^0 = \sqrt{k_F \varepsilon'/\varepsilon} = (\varepsilon'/\varepsilon)\, C_i/C^0, \quad [2]$$

where C^0 is used to normalize the defect concentration and k_F is the electrochemical mass action constant for reaction (III). The terms ε and ε' are the dielectric constants of Ag_2SO_4 and $CaSO_4$, respectively. The resultant concentration profile is shown in Fig. 6b. The enhanced interstitial divalent ion concentration in the space charge region reduces the hopping rate of mobile Ag^+ through the want of nearby vacancies. Additionally, the foreign Ca^{2+} in the space charge region at the Ag_2SO_4 surface blocks the Ag^+ mobility parallel to the interface, which

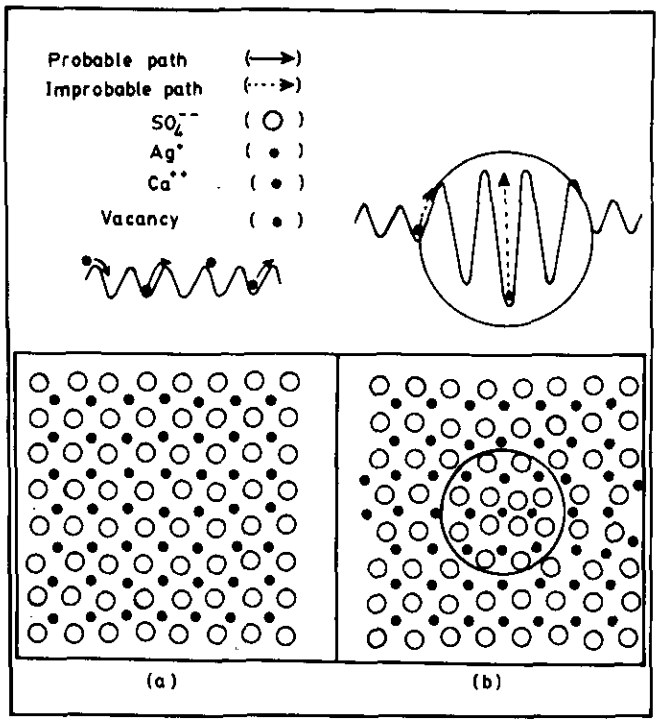

FIG. 5. Schematic representation of a plane through (a) regular host lattice with an ideal potential well and (b) lattice with some of Ag^+ replaced by Ca^{2+} with the modified potential well.

otherwise is considered as a ion percolating path (23). The overall effect is that the interfacial space charge regions are more blocking than percolating in nature; i.e., they form clusters (agglomeration of interstitial cations). The conductivity in the space charge region is normalized following the relation

$$\sigma_n = \frac{\sigma_{\text{interstitial}}}{\sigma_{\text{interior}}}. \qquad [3]$$

The variation of normalized conductivity (σ_n) with distance in the space charge layer (Fig. 6c) indicates a net fall in conductivity near the $Ag_2SO_4/CaSO_4$ interface.

CONCLUSION

Creation of vacancies by aliovalent ion substitution alone would not be sufficient, but the proper selection of ionic size is very important for conductivity enhancement, especially in low temperature phases. Furthermore, the dispersion of an improper second insoluble phase could also reduce the conductivity of a multiphase mixture. These findings throw light on the fundamental informaiton on the defect structure and in turn on the conduction mechanism in Ag_2SO_4.

APPENDIX

1. PDP11 is a powder diffraction package used to obtain the lattice parameters. It is developed by M. Calligaris and S. Geremia, Dipartimento di Scienze Chimiche, Universita di Trieste (ITALY).

2. The deviations obtained in the observed 2θ values from the standard ones (Cu target) are plotted against the corrected 2θ values. The actual deviations, hence obtained by non-linear least squares fit, are incorporated to

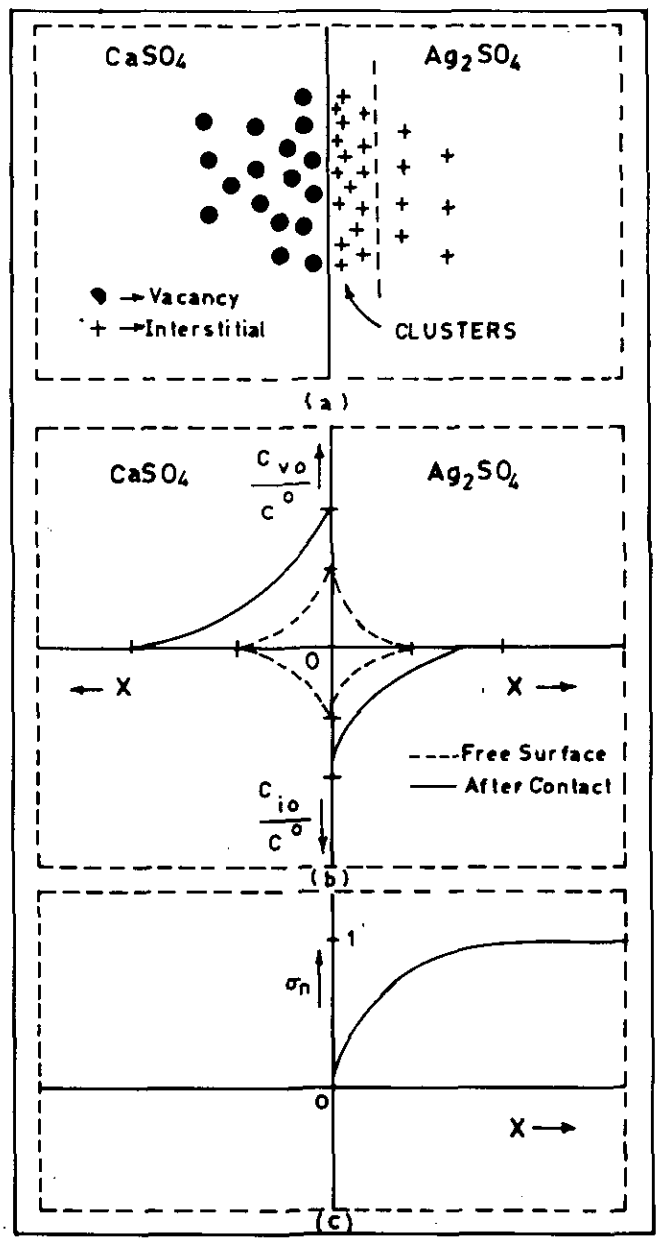

FIG. 6. Schematic representation of (a) defects at the $Ag_2SO_4/CaSO_4$ interface, (b) normalized defect concentration profile, (c) normalized conductivity variation inside the space charge region.

obtain the actual d values. The same values are fed in to the PDP11 programme to calculate the lattice parameters in the solid solubility region.

ACKNOWLEDGMENT

The authors are thankful to DOEn, New Delhi, for providing financial assistance in carrying out this work.

REFERENCES

1. H. H. Höfer, W. Eysel, and U. V. Alpen, *J. Solid State Chem.* **36,** 365 (1981).
2. K. Singh and S. S. Bhoga, *Solid State Ionics* **39,** 205 (1990).
3. K. Singh and S. S. Bhoga, *J. Solid State Chem.* **97,** 141 (1992).
4. K. Singh, S. S. Bhoga, and S. D. Wachasundar, *Appl. Phys. A* **55,** 14 (1992).
5. K. Singh and V. K. Deshpande, *Solid State Ionics* **7,** 295 (1982).
6. V. K. Deshpande, F. C. Raghuwanshi, and K. Singh, *Solid State Ionics* **18**/19,378 (1986).
7. K. Singh, V. R. Chandrayan, and V. K. Deshpande, *Solid State Ionics* **27,** 57 (1988).
8. A. R. Rodger, I. Kuwand, and A. R. West, *Solid State Ionics* **15,** 185 (1985).
9. C. C. Liang, *J. Electrochem. Soc.* **120,** 1289 (1973).
10. S. S. Bhoga and K. Singh, *Solid State Ionics* **40/41,** 27 (1990).
11. K. Singh, *Solid State Ionics* **28,** 1371 (1988).
12. M. Gauthiaer and A. Chamberland, *J. Electrochem. Soc.* **124,** 1579 (1977).
13. Q. Liu, X. Sun, and W. Wu, *Solid State Ionics* **40/41,** 456 (1990).
14. K. Singh, *Solid State Ionics* **66,** 5–14 (1993).
15. A. Kar and J. Mazumder, *J. Appl. Physics* **61,** 2645 (1987).
16. M. D. Leblanc, U. M. Gundusharma, and E. A. Secco, *Solid State Ionics* **20,** 61 (1986).
17. E. A. Secco, "Solid State Ionics: Materials and Applications," pp. 47–60. 1992.
18. J. O. Thomas and M. A. Zendejas, "Solid State Ionics: Materials and Applications," pp. 19–28. 1992.
19. A. V. N. Tilak, M. Umar, and K. Shahi, *Solid State Ionics* **24,** 121 (1987).
20. K. Shahi and J. B. Wagner, Jr., *J. Phys. Chem. Solids* **43**(8), 713 (1982).
21. S. Chaklanobis, K. Shahi, and R. K. Syal, *Solid State Ionics* **44,** 107 (1990).
22. J. Maier, *Ber. Bunsenges. Phys. Chem.* **89,** 355 (1985).
23. A. Bunde, W. Dieterich, and H. E. Roman, *Phys. Rev. Lett.* **55,** 5 (1985).